Chemical Engineering Science 247 (2022) 117091

Contents lists available at ScienceDirect

Chemical Engineering Science

journal homepage: www.elsevier.com/locate/ces

Experiments and modelling of three-phase vertical pipe flow

Jørn Kjølaas [a,*], Roel Belt [b], Marita Wolden [a], Heiner Schümann [a], Vanessa Richon [c]

[a] SINTEF Industry, Norway
[b] TotalEnergies S.E., Pôle d'Etudes et de Recherche de Lacq (PERL), Pôle Economique 2 - B.P. 47, 64170 Lacq, France
[c] TotalEnergies EP Norge AS, Finnestadveien 44, Dusavika, 4029 Stavanger, Norway

HIGHLIGHTS

- Two- and three-phase vertical flow experiments were conducted in a 50 m long vertical riser at 45 bara pressure.
- The liquid content and pressure drop were found to be highly sensitive to the water cut.
- The proposed explanation for this observation is that the presence of liquid droplets constrains the ability of the liquid to sustain small gas bubbles.
- A model was constructed to test this hypothesis, and the prevailing model predictions were found to be in good agreement with the measurements.

ARTICLE INFO

Article history:
Received 14 June 2021
Received in revised form 12 August 2021
Accepted 2 September 2021
Available online 6 September 2021

Keywords:
Vertical flow
Three-phase flow
Bubbly flow
Churn/slug flow
Experiments
Unit Cell Model

ABSTRACT

A set of two- and three-phase experiments were conducted in a 50 m long 4″ vertical pipe using nitrogen, Exxsol D60 and water at 45 bara pressure. The results show that the liquid content and pressure drop are highly sensitive to the injected water cut. The proposed explanation for this surprising result is that the presence of liquid droplets constrains the gas bubble capacity of the liquid so that the concentration of small bubbles inside the liquid becomes smaller in three-phase flows than in two-phase flows.

To test this hypothesis, a simple flow model was implemented using closure laws from the public literature, combined with the assumption that the concentration of gas bubbles is reduced by the presence of liquid droplets. The model shows that the observed three-phase effects can be reproduced very accurately using this assumption.

1. Introduction

Multiphase flow is frequently encountered in pipes and process equipment in the chemical, nuclear and oil & gas industry. In the oil & gas industry, the unprocessed fluid stream generally consists of oil, gas and water collectively flowing through pipes. The behaviour of such three-phase mixtures can be very complex, and the ability to predict the pressure drop in three-phase flows is of critical importance for the design and operation of petroleum production systems.

Deep offshore fields have vertical risers connecting the flowline on the seabed to the offshore receiving facilities, and the lengths of these risers can exceed 2000 m. For oil fields, the output is mostly liquid, and because of the hydrostatic contribution to the pressure gradient, the pressure drop over the riser is generally much larger than the pressure drop over the flowlines lying on the seabed. As a result, the back pressure on the wells, which dictates the productivity of the wells, is mostly determined by the multiphase flow in the riser. Therefore, it is of particular importance to predict the pressure drop in near-vertical flows as accurately as possible in order to (i) forecast the production and the economics of the field, or (ii) to size optimally subsea equipment, like multiphase pumps, which can be installed to boost the production.

In this paper, we will focus on two flow regimes in vertical pipes: bubbly flow and slug/churn flow. In two-phase gas–liquid flow, the pressure drop in both regimes can be predicted very well using 1D models. For instance, the pressure drop in bubbly flow can be predicted by a homogeneous flow model using a drift flux model for the slippage between the gas and the liquid (Zuber and Findlay, 1965). Drift flux models can in principle be adapted to model slug/churn flow by modifying the model coefficients appropriately (Shi et al., 2005; Pietrzak et al., 2017), but it is our view that a great deal of physical insight is lost in such an approach. This loss of insight can encumber further progress in

* Corresponding author.
E-mail address: jorn.kjolaas@sintef.no (J. Kjølaas).

https://doi.org/10.1016/j.ces.2021.117091
0009-2509/

the modelling, for instance with respect to generalizing the model to three-phase flows, which is the main topic of the present work.

The approach pursued in this paper is based on the Unit Cell Model (UCM) (Dukler and Hubbard, 1975; Fernandes et al., 1983; Fabre and Liné, 1992), which is a more rigorous method than fitting a drift flux model to the experimental data. The UCM relies on a set of closure laws, and each of these closure laws are measurable quantities that can in principle be obtained from measurements. This is a compelling benefit because it facilitates a more physically based methodology, where various physical phenomena can be modelled separately based on our knowledge and understanding of the governing mechanisms. Despite this benefit, calculating the liquid holdup from the UCM is no more difficult than calculating it in a drift flux framework, hence selecting the UCM framework for modelling churn/slug flow seems like a rational choice.

Closure laws in 1D models have been an active topic of research in the past decades, continuously yielding models with better accuracy and wider ranges of applicability (Guet et al., 2006; Kjølaas et al., 2017). For example, Kjølaas et al. (Kjølaas et al., 2017) showed that with their proposed 1D closure laws, 91% of the prevailing pressure drop predictions were within 10% of the measured values for two-phase vertical flows with low liquid viscosity (0.3–2 cP). Here, the examined data set consisted of 845 data points with gas densities ranging from 25 to 100 kg/m^3.

As mentioned above, oil wells generally produce oil, gas and water at the same time, hence the flow in most deep-water risers is three-phase, and not two-phase. Consequently, although two-phase flows are important special cases with respect to multiphase flow modelling, models must ultimately be able to adequately deal with three-phase flows because this is the most common scenario.

There are only a few experimental studies on vertical three-phase pipe flow in the literature, and all the studies were conducted in low-pressure systems. For example, Descamps et al. (Descamps et al., 2007) conducted vertical three-phase experiments using two different oils with viscosities 3.1 and 7.5 cP. The results showed that the total pressure drop generally increased with the water cut, except around the phase inversion point in certain scenarios. Three-phase holdups were unfortunately not measured; hence it was difficult to deduce the mechanisms responsible for the observed pressure drop variations.

Colmanetti et al. (Colmanetti et al., 2018) conducted vertical three-phase experiments using a 23 cP oil. The pressure drop was found to have a maximum around the phase inversion point, while the liquid holdup did not vary significantly with water cut. Consequently, the primary mechanism responsible for the pressure drop variation was presumably the rheology of the oil/water mixture.

Xu et al. (Xu et al., 2012) conducted vertical three-phase experiments using a 44 cP oil and found that the liquid holdup increased with water cut up to the inversion point, and then gradually decreased as the water cut approached 100%. This behaviour is consistent with the experimental findings presented in this paper.

Very little modelling work has been reported in vertical three-phase bubbly and slug flow. It is worth noting that Fernandes et al. (Fernandes et al., 1983) successfully used the same approach (UCM) as deployed in this paper to predict two-phase vertical flows. Except for the gas entrainment model, the closure laws that they used were similar to those used here, and they were able to match the measured liquid fractions within 5%.

Frechou (Frechou, 1986) is the only author to our knowledge who has tested the UCM framework on a vertical three-phase flow data set. He showed that a two-phase gas–liquid UCM was able to recover very well the measured gas holdup and pressure drop in three-phase flow, since the oil and water behaved like a homogeneous liquid phase. His main modelling issue was the rheology model to predict the Taylor bubble velocity, which in the UCM determines to a large extent the gas holdup in the pipe. Because of the small pipe diameter (0.054 m) and the dense emulsion, the Reynolds number in the liquid slug was in or below the laminar-turbulent transition regime for most data points and therefore the emulsion rheology impacted the Taylor bubble velocity significantly. Specifically, the emulsion behaved like a shear-thinning fluid, making the velocity profile in the liquid slug flatter than for a Newtonian fluid. Since the liquid velocity on the vertical axis partly defines the Taylor bubble velocity (Collins et al., 1978; Boucher et al., 2021), the flatter velocity profile could explain according to (Frechou, 1986) the observed decrease of the Taylor bubble velocity compared to a Newtonian fluid. In oil & gas field cases, however, the liquid slug is generally fully turbulent and the emulsion rheology should have a much smaller impact on the Taylor bubble velocity (as was the case for the data points in (Frechou, 1986) at the highest Reynolds numbers).

Frechou's approach of modelling the oil/water mixture as a homogeneous liquid phase is in our view reasonable, and we justify this view in Section 3.2 in this paper. Still, analyses of field data with risers have indicated that applying a regular two-phase model on three-phase systems leads to a systematic underprediction of the pressure drop (see Section 4). In long risers, even moderate errors can give large absolute errors in the well head pressure, which has large implications on the forecast of the well productivity. Consequently, because the pressure drop predictions in vertical pipes can have such a large influence on the total pressure drop, model improvements for three-phase vertical flows were deemed necessary.

To understand the discrepancies observed when comparing predictions to field measurements, a set of two- and three-phase flow experiments were conducted in a 4″ vertical pipe at high pressure (45 bara). The setup and the experimental results are described in Section 2. In Section 3 we show that standard two-phase gas–liquid models predict the pressure drop in two-phase experiments very well, but underpredict the pressure drop in our three-phase flow significantly, which was consistent with the field data observations. To improve the situation, we propose a simple modification of the void-in-slug model in three-phase flow, based on some physical considerations. With this change, we demonstrate that the pressure drop for the three-phase data is reproduced very well. Next, in Section 4, we show that this change allows us to recover the pressure drop in field data. Finally, in Section 5, we provide some concluding remarks about our work.

2. Experiments

In this section we describe the experimental setup and procedures used to conduct the experiments.

2.1. Experimental setup

The experiments were conducted using a 50 m vertical pipe with internal diameter 97.18 mm (4″), and a wall roughness of 5 μm. The setup is illustrated below, next to the instrument list (Table 1). Nitrogen, Exxsol D60 and tap water were injected at the bottom of the pipe, flowed through the pipe, ultimately ending up in a large three-phase gravity separator. Coriolis meters were used to measure the flow rates and fluid densities. The pipe was instrumented with eight pressure-transmitters (labelled P) that were coupled to a common gas-filled reference line, five single energy narrow-beam gamma densitometers (logged at 50 Hz) for estimating liquid fraction and calculating the velocity of large waves/slugs (labelled γ), and one laterally scanning gamma densitometer (single energy) for measuring density profiles and slice averaged density (phase fractions) (labelled γ_T). In addition, a

Table 1
Instrument list.

Label	Type	Location
γ_1	Gamma densitometer	6.51
T_1	Temperature transmitter	7.82
P_1	Pressure transmitter	8.72
P_2	Pressure transmitter	17.34
QCV	Quick-closing valve	24.35
γ_2	Gamma densitometer	25.15
P_3	Pressure transmitter	25.95
P_4	Pressure transmitter	30.97
γ_3	Gamma densitometer	32.01
P_5	Pressure transmitter	34.56
γ_4	Gamma densitometer	37.60
P_6	Pressure transmitter	38.87
γ_T	Traversing gamma densitometer	40.68
P_7	Pressure transmitter	42.99
γ_5	Gamma densitometer	43.37
P_8	Pressure transmitter	47.48
T_2	Temperature transmitter	50.21

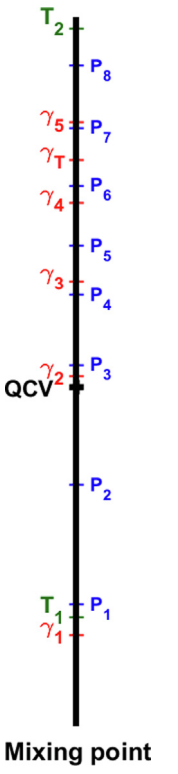

26.65 m long shut-in section for measuring average phase fractions with high accuracy was included. The quick-closing valve used to shut in the fluids is labelled QCV in Table 1. Finally, temperature transmitters (labelled *T*) were mounted at the beginning and end of the test section. The experiments were performed at 45 bara pressure and 20 °C, yielding a gas density of approximately 52 kg/m^3.

2.2. Fluid system

The thermodynamic properties if the fluids are listed in Table 2. The gas and water properties were calculated using NIST reference data (National Institute of Standards and Technology, xxxx), while the oil density and viscosity were obtained using Coriolis meter and rheometer measurements. The surface tension values listed in Table 2 were obtained by conducting pendant drop measurements. For gas/water and oil/water, a range of values is provided in the table. In these cases, the measured surface tension varied significantly over time, starting off at a high value and later levelling off at a lower value after a period of 15–30 min. The reason for this time dependency is believed to be related to the presence of surfactants that slowly migrate from the bulk fluid to the interface over time. For the sake of the flow experiments, we believe that the most relevant surface tension values are the initial ones, so we have used the highest values in the modelling described in Section 3. The reason for this is that in multiphase flows, new interfaces are continuously created and destroyed, and the lifetimes of interfaces are presumably short compared to the diffusion time scale.

Table 2
Fluid properties at 45 bara pressure and 20 °C.

	Gas	Oil	Water
Density [kg/m^3]	52.1	785.6	1000
Viscosity [cP]	0.018	1.36	1.01
	Gas/oil	**Gas/water**	**Oil/water**
Surface tension [mN/m]	26	51–76	22–55

The inversion point of the oil/water dispersions formed by the fluids was determined in a special mini-loop setup. Here, oil–water mixtures at known water cut (*WC*) were dispersed in a mixing valve before entering a horizontal steel tube of 8 mm inner diameter and 2 m length. For reference, this setup was similar to the one applied by Pal in his rheology study (Pal, 1993). A pressure drop of 1 bar over the mixing valve was used to create droplets with sizes of the order of a few micrometers. Pressure drop measurements over the mini-loop test section are shown in Fig. 1 for mixture velocities of 1.0 and 1.5 m/s. A typical dispersion behaviour can be observed where the pressure drop increases drastically towards a peak marking the phase inversion point of the system. At phase inversion the dispersed system changes its continuity from oil continuous flow with dispersed water droplets to water continuous flow with dispersed oil droplets. The measurements indicate that this happens at around 40% WC. The higher pressure drop in this region is caused by an effective dispersion viscosity which can be considerably higher than the pure phase viscosities. The nonlinear behaviour on both sides on the inversion point is caused by the transition between laminar and turbulent flow, where laminar flow prevails as the inversion point is approached.

2.3. Instruments and measurements

In the following paragraphs we briefly describe the most important instruments/measurements used in this campaign, and the associated measurement uncertainties. The reported uncertainties are expressed as one standard deviation.

2.3.1. Pressure gradient

Pressure gradients were calculated using all the pressure transmitters (logged at 2 Hz) on the test section except for the first and last (P_1 and P_8 were omitted). The reason for excluding these was to evade possible inlet/outlet effects. The pressure was measured using differential pressure sensors that measured pressure relative to a gas-filled reference line. The gradient and the associated uncertainty were calculated by linear regression of the pressure readings versus pressure tap position. The typical uncertainty in the pressure gradients was found to be 0.8%.

2.3.2. Static gamma densitometers

Five single energy narrow-beam gamma densitometers were distributed along the riser. All the gamma densitometers consisted of a Caesium radiation source on one side of the pipe and a photon detector on the other side. The attenuation of the photon beam decreases exponentially with the density of the medium between the source and detector, allowing us to measure the average density along the rays' travel path. In two-phase flows, we can translate the measured densities into phase fractions along the photon beams. All the gamma densitometers were logged at 50 Hz.

The gamma densitometers were collimated on both the source side and the detector side. With this type of arrangement, scattered photons rarely reach the detector, and the prevailing phase fraction accuracy has been shown to be about 0.01 for two-phase gas–liquid systems. It is important to note that the measured phase fractions are not necessarily representative of the actual volume fractions, because these instruments only measure along the centreline. Also, in three-phase flows, phase fractions cannot be calculated from these measurements without additional assumptions. Therefore, in the three-phase experiments conducted in this

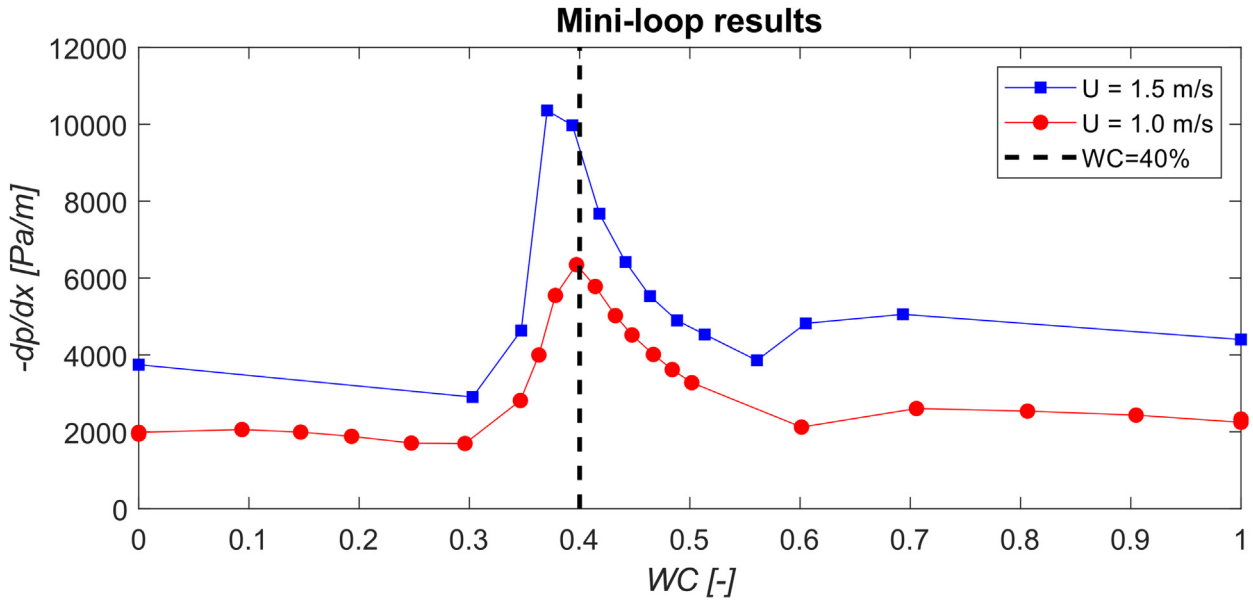

Fig. 1. Pressure drop plotted versus water cut for two different flow velocities (1.0 and 1.5 m/s) in the mini-loop.

campaign, we imposed the assumption of zero slip between oil and water to calculate the associated line fractions. These measurements were however not used to calculate holdups reported in this paper, as the primary purpose of these instruments was to monitor the flow development along the riser and assess whether the flow appeared to be fully developed. In all the experiments presented here, the flow appeared to always be fully developed downstream the second gamma densitometer.

In the experiments in the churn/slug flow domain, the last two gamma densitometers were also used to estimate the propagation velocities of the slugs. This is described in more detail in Section 2.4.2.

2.3.3. Traversing gamma densitometer

One traversing gamma densitometer (single-energy gamma instrument) was installed near the top of the riser. This instrument was the same type of instruments as the static gamma densitometers, but it was mounted on a mechanical traversing device that allowed the photon beam to scan the entire pipe. The velocity of the traversing device was 0.2 mm/s. This instrument was used to measure average (slice-averaged) density profiles, which can be integrated to find the associated phase fractions in two-phase flows. The uncertainty in the phase fraction measurements was estimated to be about 0.01.

In three-phase flows, the phase fractions cannot be unambiguously derived from the density profiles, so in those cases a shut-in system was used to measure the phase fractions, see Section 2.3.4.

2.3.4. Shut-in section

A quick-closing valve was installed 26.65 m from the top of the riser so that the top part of the riser worked as a shut-in section. The purpose of this shut-in section was to measure average phase fractions in three-phase flows. The system was operated as follows:

* When the system had reached steady state, and the other measurements had been completed, the shut-in valve was closed, and the liquids above the valve could settle and separate.
* The liquid above the shut-in valve was then drained through a Coriolis meter, which measured both the mass rate and the density of the drained fluids.
* The density measurement was used to distinguish between oil and water, and the mass rate measurement was used to measure the total mass of each phase. The volume of each phase was then found by dividing the oil/water masses by the respective densities.
* The oil and water holdups were obtained by dividing the oil/water volumes by the total volume downstream the valve.

The uncertainty in these fraction measurements was estimated to be less than 0.01.

2.4. Results

The experimental conditions mainly cover two superficial gas velocities: *USG* = 1 and 2 m/s, four superficial liquid velocities: *USL* = 0.5, 1, 1.5 and 2 m/s, and six water cuts: *WC* = 0, 20, 40, 60, 80, 100%. These experiments were all determined to be in the bubbly/slug/churn flow domain, and not in the annular flow region. It should be noted that since the pipe was not transparent, the flow regime determination is uncertain, and we have not made any attempt to classify the different points aside from excluding annular flow on the grounds of observing relatively high average liquid fractions. The reason for making this particular distinction is that we will in Section 3 propose a model that is suitable for bubbly/slug/churn flow, but unsuitable for annular flows.

We should also point out that the distinction between churn flow and slug flow is generally unclear, as definitions of churn flow vary in the literature (Hewitt and Jayanti, 1993). Also, under certain definitions, these two flow regimes have similar characteristics (Mao and Dukler, 1993; Taitel et al., 1980), making it difficult to distinguish between them experimentally. In this paper we will treat these two flow regimes as one and the same. We define this common churn/slug flow regime by positing the coexistence of large Taylor-like bubbles with sizes in the order of the pipe diameter or larger, and small millimetre-sized dispersed bubbles. In other words, our definition of churn flow does not encompass churn/annular flow with a continuous gas core. This definition of churn flow is partially motivated by the modelling proposed in Section 3, where we need to construct a somewhat simplistic view of the churn/slug flow regime, even though the reality may be more complex.

2.4.1. Pressure drop and phase fractions

Fig. 2 shows 3x2 graphs that contain the experimental results in terms of the pressure drop, liquid fraction and the intrinsic water fraction (the water fraction divided by the liquid fraction), which are plotted versus the water cut. The graphs on the left show results for *USG* = 1 m/s, and the graphs on the right show results for *USG* = 2 m/s. In the top graph, we have included values for the total pressure drop (markers), and the gravitational pressure drop (dashed lines). The gravitational pressure drop was calculated from the measured phase fractions:

$$-\left(\frac{dp}{dx}\right)_{grav} = \left(\alpha_g\rho_g + \alpha_o\rho_o + \alpha_w\rho_w\right)g \quad (1)$$

The experimental data shown in these graphs are provided in tabulated form in Table 4 in Appendix A.

In the top graphs we observe that the total pressure drop and the gravitational pressure drop are very similar in these experiments, which means that friction plays only a minor role. Because of this, we exclusively focus on the phase fractions in the modelling proposed in Section 3.

The most notable observation in these results is that the liquid holdup depends significantly on the water cut. Specifically, the liquid fraction is always higher in three-phase flows than in two-phase gas/liquid flows when the gas- and liquid superficial velocities are the same. The maximum liquid fraction is in almost all cases observed at *WC* = 40%. Incidentally, as shown in Section 2.2, the mini-loop experiments conducted with this oil/water mixture showed that the phase inversion point was around 40%, suggesting that the observed liquid fraction may be related to that. It should however be pointed out that the typical magnitude of the liquid Reynolds number in these experiments was around 10^5, and the

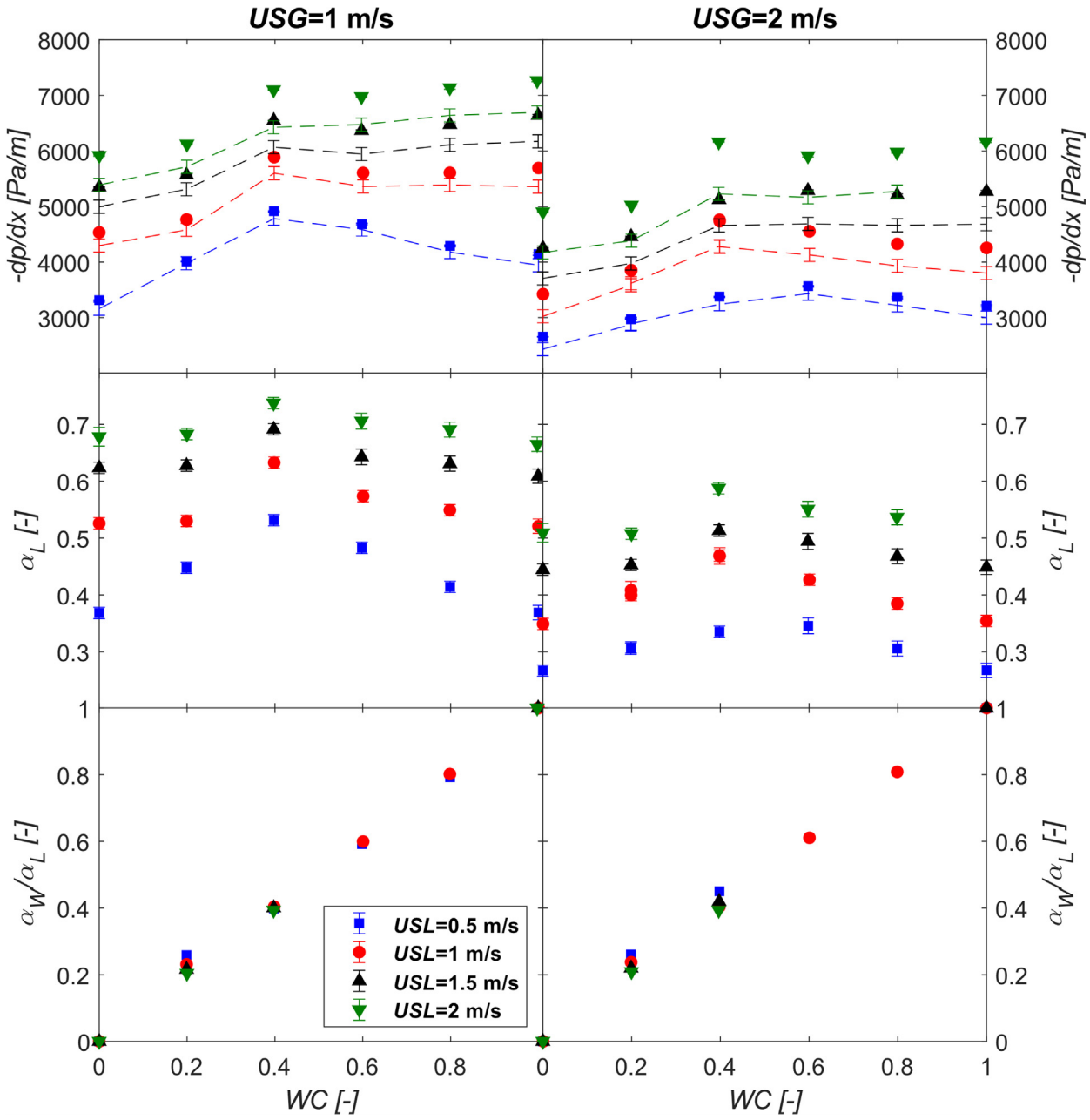

Fig. 2. Measured pressure drop, liquid holdup and intrinsic water fraction plotted versus water cut for *USG* = 1 and 2 m/s, and *USL* = 0.5–2 m/s. The dashed lines in the top graph show the gravitational pressure drop.

liquid fraction is thus not expected to be sensitive to the liquid viscosity. Consequently, although the effective liquid viscosity in the three-phase flow cases may be higher than in two-phase flows, we do not believe that the trends observed for the liquid fraction can be attributed to this effect.

In the top graphs of Fig. 2 we see that the trends that we observe for the liquid fraction are reflected in the pressure drop results. This is because the total pressure drop is mainly a product of the gravitational component in these experiments. In fact, the gravitational component of the pressure drop was typically around 90% of the total pressure drop in these experiments, hence the ability of models to predict the liquid fraction in such cases is critical. At high water cuts, the trends in the pressure drop are a bit different compared to the liquid fraction, appearing "flatter". This is simply because water is heavier than oil, so that the liquid fraction variation is to a certain extent cancelled by the increased liquid weight in the pressure drop trends.

The bottom graphs in Fig. 2 show that intrinsic water fraction is for the most part quite close to the water cut, and this means that the oil and water travel at approximately the same velocity. This is consistent with the findings by Frechou (Frechou, 1986). For a few of the points at moderate water cuts ($\leq$40%) and moderate superficial liquid velocities ($USL \leq 1$ m/s), we do observe that the water fraction is slightly higher than the water cut, but the deviation from "no-slip" is not very large. More importantly, it seems clear that the trends observed in the liquid fraction are not correlated with the oil/water slip velocity. Specifically, at high water cuts, there is no measurable oil/water slip, but we still observe large variations in the liquid fraction. Consequently, the three-phase effects observed for the liquid fraction can arguably not be attributed to oil/water slip effects.

The thesis of this paper is that the three-phase effects observed for the liquid fraction can be attributed to changes in the concentration of small gas bubbles inside the liquid. Specifically, we believe that the presence of liquid droplets dispersed in the continuous liquid phase reduces the liquid's capacity for storing small gas bubbles, causing a decrease in the bubble concentration. In churn/slug flow, this phenomenon ultimately leads to an increase in liquid holdup in three-phase flows, as will be shown in Section 3.2.

2.4.2. Slug bubble velocities

As explained previously, the churn/slug flow regime is characterized by the existence of both large Taylor-like bubbles and small bubbles. Fig. 3 shows some measurements from an experiment in the churn/slug flow regime, where the liquid centre-line fraction at two locations is plotted versus time. In this graph we observe that the measured liquid fraction typically varies between 0.2 and 0.45. Our interpretation of these results is that the periods with low liquid fraction represent Taylor-like bubbles, while the high liquid fractions represent slugs. If we assume that the centre-line fraction equals the volumetric fraction, we may infer from this graphs that the concentration of small gas bubbles in the slugs is around 55%.

The blue line in Fig. 3 shows the liquid fraction measured at 37.60 m from the inlet, while the thin black line shows the liquid fraction measured 5.77 m downstream. The red curve is the same as the black curve, but the signal has been shifted by 2.84 s to "match" the blue curve as closely as possible. The value of 2.84 s was obtained using a generic cross-correlation algorithm. We observe that the red and blue curves match reasonably well, suggesting that the large Taylor-like bubbles travel at approximately the same velocity. The average velocity of these bubbles can be estimated by dividing the distance between the measurements (5.77 m) by the cross-correlation lag (2.84 s), yielding a value of 3.46 m/s.

This procedure was carried out for all the experiments where a good cross-correlation was achievable. In many cases, a good cross-correlation was not achievable either because the flow changed too much between the measurement points, or because the flow structures were too small and complex. The prevailing velocities for the experiments for which we were able to apply this analysis are shown in Fig. 4, where we have plotted the slug velocity against the mixture velocity U_M. In this plot we have also included predictions obtained using the Nicklin bubble velocity model (Nicklin et al., 1962), which for vertical flow in large diameters is given by:

$$U_B = 1.2 \cdot U_M + 0.35 \cdot \sqrt{\frac{\left(\rho_l - \rho_g\right) gD}{\rho_l}} \tag{2}$$

Here, U_M is the mixture velocity, D is the pipe diameter, g is the gravity acceleration, ρ_g is the gas density, and ρ_l is the liquid density. This model is generally valid for high Reynolds numbers and high Bond numbers, both of which are satisfied for our data set (see Table 3). We see in Fig. 4 that the overall agreement between this simple model and the measured velocities is reasonable for both two-phase and three-phase flows. In fact, we do not see any evidence that the slug velocity is different in two- and three-phase flows, which is an important observation with respect to the model derivation proposed in Section 3.2. It is difficult to assess the effective uncertainty in these velocity estimates, but we suspect that the observed discrepancies between the model and measurements could at least partially be caused by uncertainties prevailing from the analysis.

The data shown in Fig. 4 are tabulated in Table 3. In this table we have included the slug Reynolds numbers *Re* and the Bond numbers *Bo* for each case. The definition of these numbers are:

$$Re = \frac{\left(\alpha_L \rho_L + \alpha_G^s \rho_G\right) \cdot D \cdot U_M}{\mu_L} \tag{3}$$

$$\mathrm{Bo} = \frac{(\rho_L - \rho_G) g D^2}{\sigma} \tag{4}$$

The definitions of the various parameters in these expressions can be found in Section 3.

3. Modelling

As stated in Section 2.4.1, the gravitational component typically accounts for around 90% of the total pressure drop in our experiments. Consequently, a model's ability to predict the liquid fraction is by far the most critical aspect, while predicting the frictional pressure drop is secondary. For this reason, the modelling efforts presented here focus on predicting the liquid fraction.

3.1. Two-phase flows

In this section we present a model for two-phase vertical bubbly/slug/churn flow based on the closure laws proposed by Kjølaas et al. (Kjølaas et al., 2017). These closure laws were based on experiments conducted at conditions that are similar to those in the present experiments, although the former data set only included two-phase gas/oil flows.

3.1.1. Bubbly flow

Bubbly flow is described as a liquid continuous flow, where the gas is present in the form of small bubbles dispersed in the liquid phase. In this regime, the only closure law required to calculate the liquid holdup is the slip velocityΔubetween the bubbles and the liquid. The slip velocity of bubbles rising in liquid generally depends on the bubble size. However, the typical size range for the bubbles in these types of flows is reported to be 1–6 mm

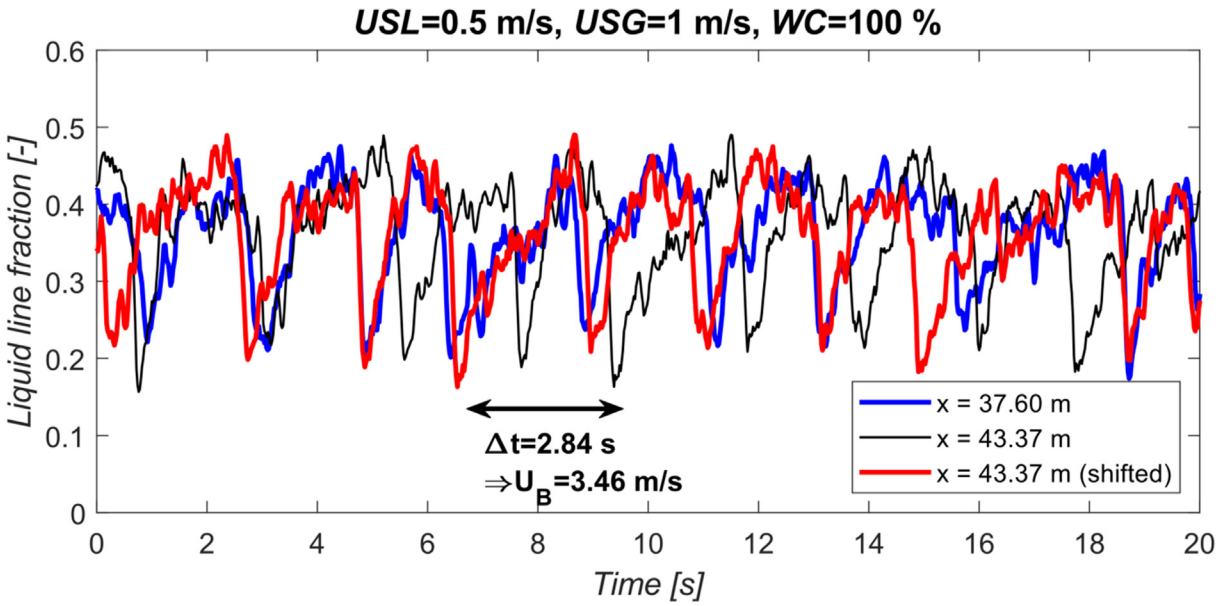

Fig. 3. Liquid centre line fraction measured at two locations plotted versus time. The red curve has been shifted by 2.84 s to match the blue curve. (For interpretation of the references to colour in this figure legend, the reader is referred to the web version of this article.)

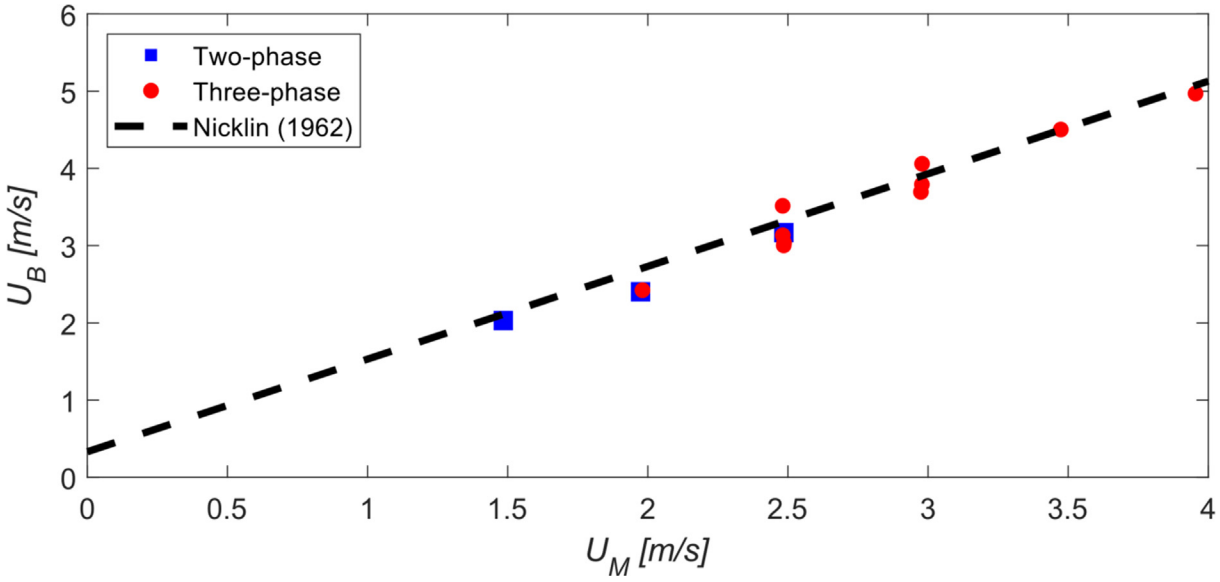

Fig. 4. Measured cross-correlation velocity plotted versus the mixture velocity. Blue squares: two-phase flow, red circles: three-phase flows. The black line represents the Nicklin model (Nicklin et al., 1962) which is provided in Eq. (2). (For interpretation of the references to colour in this figure legend, the reader is referred to the web version of this article.)

(Krishna and Wilkinson, 1991; Krishna, 2000), which according to Harmathy (Harmathy, 1960) is in a size range where the slip velocity is relatively insensitive to the bubble/droplet size. For this size range, Harmathy found that the following model applies:

$$\Delta u_H = 1.53 \cdot \left(\frac{\sigma g |\Delta\rho \sin\phi|}{\rho_L^2} \right)^{1/4} \tag{5}$$

Here, we have definedΔu_Has the "Harmathy slip velocity". It is important to point out that the Harmathy model predicts the slip velocity for single bubbles, while in bubbly flows, we need to predict the average slip velocity of swarms of bubbles. Swarms of bubbles rise slower than single bubbles because of hindrance effects, and this needs to be accounted for appropriately. Kjølaas et al. (Kjølaas et al., 2017) showed that the measured rise velocity of bubble swarms could be reproduced by introducing a Richardson-Zaki (Richardson and Zaki, 1954) type of correction to the Harmathy model:

$$\Delta u = \alpha_L^n \cdot \Delta u_H \tag{6}$$

where the best fit to the data was obtained by selecting $n = 0.9$. This is reasonably comparable to the exponents suggested for gas bubbles by Ishii & Zuber (Ishii and Zuber, 1979) ($n = 0.75$) and Zuber & Findley (Zuber and Findlay, 1965) ($n = 0.5$).

With this closure model, it is a relatively straightforward exercise to calculate the liquid holdup in bubbly flow, by solving the following equation:

$$\alpha_L^{0.9} \cdot \Delta u_H = \frac{USG}{1-\alpha_L} - \frac{USL}{\alpha_L} \tag{7}$$

Table 3
Table containing slug bubble velocity data: Superficial gas velocity *USG*, superficial liquid velocity *USL*, water cut *WC*, slug Reynolds number *Re*, Bond number *Bo*, slug bubble velocity U_B.

USG [m/s]	USL [m/s]	WC [-]	Re [-]	Bo [-]	U_B [m/s]
0.991	0.990	0.398	114,402	2900	3.06
0.991	0.983	1.000	80,729	1165	2.82
0.993	0.492	1.000	65,641	1165	3.46
1.981	1.973	0.396	203,389	2896	6.11
1.985	0.994	0.601	198,560	1061	6.45
1.985	0.990	0.398	161,009	2900	5.24
1.986	1.488	0.199	121,082	2748	4.65
1.986	0.991	0.199	107,797	2748	4.04
1.987	0.495	0.598	169,500	1060	3.60
1.987	0.494	0.799	135,089	1113	3.86
1.989	0.497	0.198	92,428	2748	3.63
1.989	0.496	0.199	92,634	2749	3.83
1.989	0.496	0.000	61,612	2599	3.47

This equation does not have a closed form solution for the liquid fraction α_L, but it is straightforward to find a numerical solution using an iterative approach. This model only accounts for the gravitational drift of the bubbles and thus implicitly assumes that the bubbles are distributed homogeneously in the pipe cross section. As we see in Fig. 5, the liquid fraction profiles obtained in the bubbly flow experiments conducted in this campaign support this notion. Here we observe that the measured liquid fractions are close to homogeneous, hence is it not necessary to account for "distribution slip" in the bubbly flow drift flux model.

3.1.2. Churn/slug flow

In vertical flows, bubbly flow can only prevail up to a certain critical gas fraction (Kjølaas et al., 2017; Krishna and Wilkinson, 1991; Taitel et al., 1980). When this critical gas fraction is exceeded, small bubbles start to coalesce into larger bubbles, and the resulting flow regime is no longer accurately described by the regular bubbly flow model. Indeed, the prevailing regime is usually referred to as churn/slug flow. This regime may be viewed as a special form of bubbly flow, where the special feature is that it has a more heterogeneous distribution of bubble sizes than regular bubbly flow. This feature greatly increases the complexity of the flow, but it was shown by Krishna & Wilkinson (Krishna and Wilkinson, 1991) and Kjølaas et al. (Kjølaas et al., 2017) that this regime can be described reasonably well by dividing the bubble sizes into two main classes: Small bubbles like those encountered in bubbly flow, and large Taylor bubbles which typically have sizes of several pipe diameters or more. By ascribing suitable velocity models for the two bubble size classes, the modelling problem reduces to that of steady-state slug flow, which can be described by the well-known Unit Cell Model (UCM) equations (Dukler and Hubbard, 1975). A schematic description of the Unit Cell Model and the associated parameters is shown in Fig. 6.

In the UCM, the average gas fraction α_G^{UCM} is given by:

$$\alpha_G^{UCM} = SF \cdot \alpha_G^S + (1 - SF) \cdot \alpha_G^B \tag{8}$$

where α_G^S is the gas fraction in the slugs, α_G^B is the gas fraction in the slug bubbles, and *SF* is the slug fraction ($SF = L_S/(L_S + L_B)$). Similarly, mass conservation demands that the global superficial gas velocity *USG* equals the weighted average of the superficial gas velocities in the unit cell.

$$USG = SF \cdot USG^S + (1 - SF) \cdot USG^B \tag{9}$$

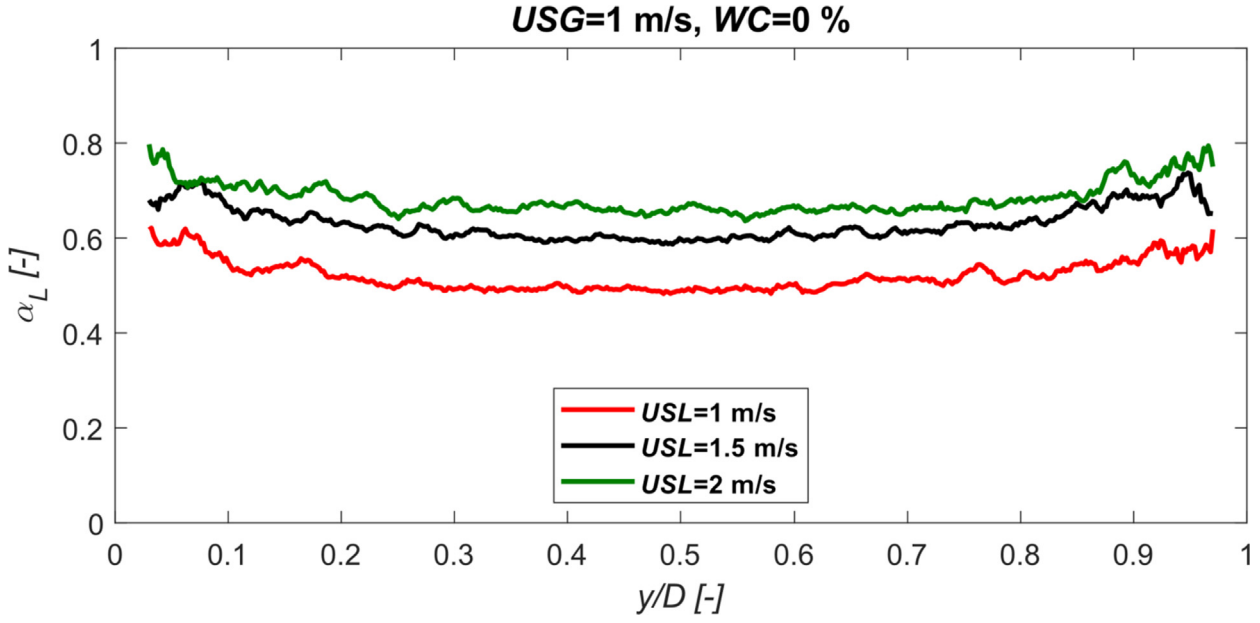

Fig. 5. Local liquid fraction plotted versus normalized distance from the wall for experiments in the bubbly flow region. The measurements were conducted using the traversing gamma densitometer described in Section 2.3.3.

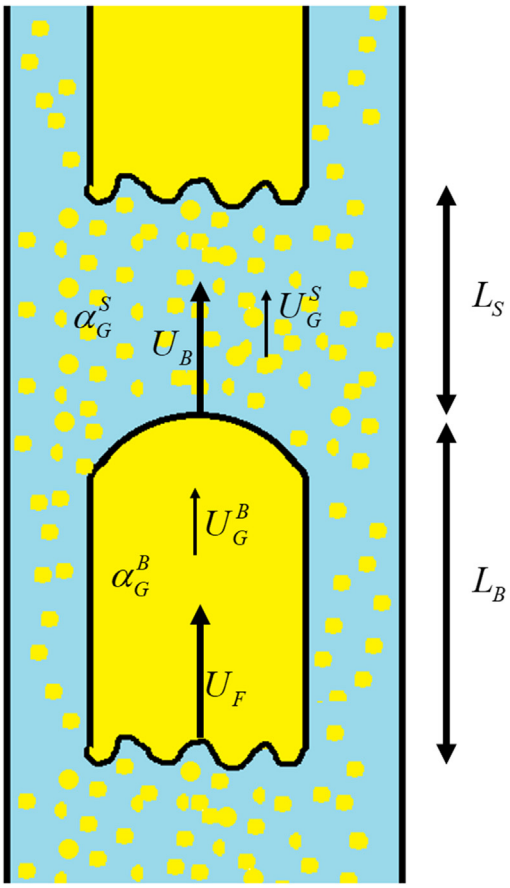

Fig. 6. Schematic description of the Unit Cell Model (UCM). Here, U_B is the bubble nose velocity, U_F is the slug front velocity, U_G^B is the gas velocity in the slug bubble, U_G^S is the gas velocity in the slug, α_G^B is the gas fraction in the slug bubble, and α_G^S is the gas fraction in the slug. L_S and L_B are the slug- and bubble lengths.

Here, USG^S and USG^B are the superficial gas velocities in the slug and slug bubble, respectively. Finally, mass conservation over the slug front in the unit cell yields the following equation:

$$\alpha_G^B\left(U_F - U_G^B\right) = \alpha_G^S\left(U_F - U_G^S\right) \tag{10}$$

where U_F is the slug front velocity, U_G^B is the gas velocity in the slug bubble, and U_G^S is the gas velocity in the slug. In steady-state fully developed flow, the average slug front velocity U_F may be assumed to equal the average slug tail velocity U_B. In addition, we have by definition that $\alpha_G^B U_G^B = USG^B$ and $\alpha_G^S U_G^S = USG^S$, hence Eq. (10) can be rearranged to yield the following expression for USG^B:

$$USG^B = USG^S + U_B(\alpha_G^B - \alpha_G^S) \tag{11}$$

We now substitute Eq. (11) into Eq. (9), yielding:

$$USG = SF \cdot USG^S + (1 - SF) \cdot \left[USG^S + U_B(\alpha_G^B - \alpha_G^S)\right] \tag{12}$$

Some trivial rearrangements of Eq. (12) gives the following expression:

$$USG = USG^S - U_B\alpha_G^S + U_B\left[SF \cdot \alpha_G^S + (1 - SF) \cdot \alpha_G^B\right] \tag{13}$$

Here, we recognize that the expression inside the last parentheses is the same as the right-hand-side of Eq. (8). Consequently, by substituting Eq. (8) into (13), we may write:

$$USG = USG^S - U_B\alpha_G^S + U_B\alpha_G^{UCM} \tag{14}$$

Finally, we rearrange Eq. (14) and use the identity $USG^S = \alpha_G^S U_G^S$ to obtain an expression for α_G^{UCM}:

$$\alpha_G^{UCM} = \frac{USG + \alpha_G^S\left(U_B - U_G^S\right)}{U_B} \tag{15}$$

From Eq. (15), we may conclude that to calculate the average gas/liquid fractions in the UCM, we only need three closure laws:

The velocity of the gas bubbles inside the slugs U_G^S.
The slug bubble velocity U_B.
The gas fraction in the slugs α_G^S.

It is worth noting that to calculate the average gas fraction α_G^{UCM}, no information is needed about the flow between the slugs, such as the concentration of bubbles in the liquid film, or liquid droplets in the gas core. This is rather convenient because the flow between the slugs is difficult to both measure and model accurately.

The velocity of the gas bubbles inside the slugs U_G^S can be calculated using the same closure law as in bubbly flow, as outlined in Section 3.1.1. Indeed, using the same slip relation in the slugs as in bubbly flow yields a continuous flow regime transition, which is consistent with experiments (Kjølaas et al., 2017). The prevailing expression for the velocity of the gas bubbles in the slugs U_G^S can be found from the definition of the slip velocity Δu:

$$\Delta u = U_G^S - U_L^S = U_G^S - \frac{USL^S}{1 - \alpha_G^S} \tag{16}$$

Multiplying this equation with $1 - \alpha_G^S$ and using the identity $U_M = USL^S + USG^S$ ultimately leads to the following expression:

$$U_G^S = U_M + (1 - \alpha_G^S)\Delta u = U_M + (1 - \alpha_G^S)^{1.9}\Delta u_H \tag{17}$$

As we showed in Section 2.4.2, the slug bubble velocity U_B can be adequately modelled using the Nicklin model (Nicklin et al., 1962) described by Eq. (2), because of the large liquid Reynolds- and Bond numbers. Consequently, we elect to use that simple expression here, even though more advanced models are available (Kjølaas et al., 2017; Joseph, 2003; Boucher et al., 2021). Finally, to predict the slug gas fraction, we use the model proposed in (Kjølaas et al., 2017):

$$\alpha_G^S = 0.6\left(1 - e^{-21.5\frac{\rho_G}{\rho_L}}\right)^{0.6} + 0.1 \cdot \sqrt{\frac{U_B - U_M}{\left(\frac{\sigma g|\Delta\rho \sin\phi|}{\rho_L^2}\right)^{1/4}} - 4} \tag{18}$$

The first part of this expression is an empirical model that describes how closely gas bubbles can be packed in stagnant liquid before coalescing into Taylor-like bubbles. Specifically, it may be interpreted as the transition point (critical gas fraction) between bubbly flow and churn/slug flow in stagnant liquid. This is the most important contribution for high gas densities, where bubbles can be packed very densely before coalescing. This model constituent is based on experiments reported by Krishna & Wilkinson (Krishna and Wilkinson, 1991) and Kjølaas et al. (Kjølaas et al., 2017), who performed bubble column experiments in static/near-static liquid at different pressures, examining at which conditions the transition between bubbly flow and churn flow took place.

The last term in Eq. (18) accounts for the notion that gas bubbles can be more closely packed in a flowing situation than in a static situation. As explained in (Kjølaas et al., 2017), the strong mixing at the slug front generates smaller bubbles, facilitating more effective bubble packing and subsequently larger gas fractions.

A comparison of Eq. (18) with measurements is shown in Fig. 7. In the left graph, Eq. (18) is compared to measurements in stagnant

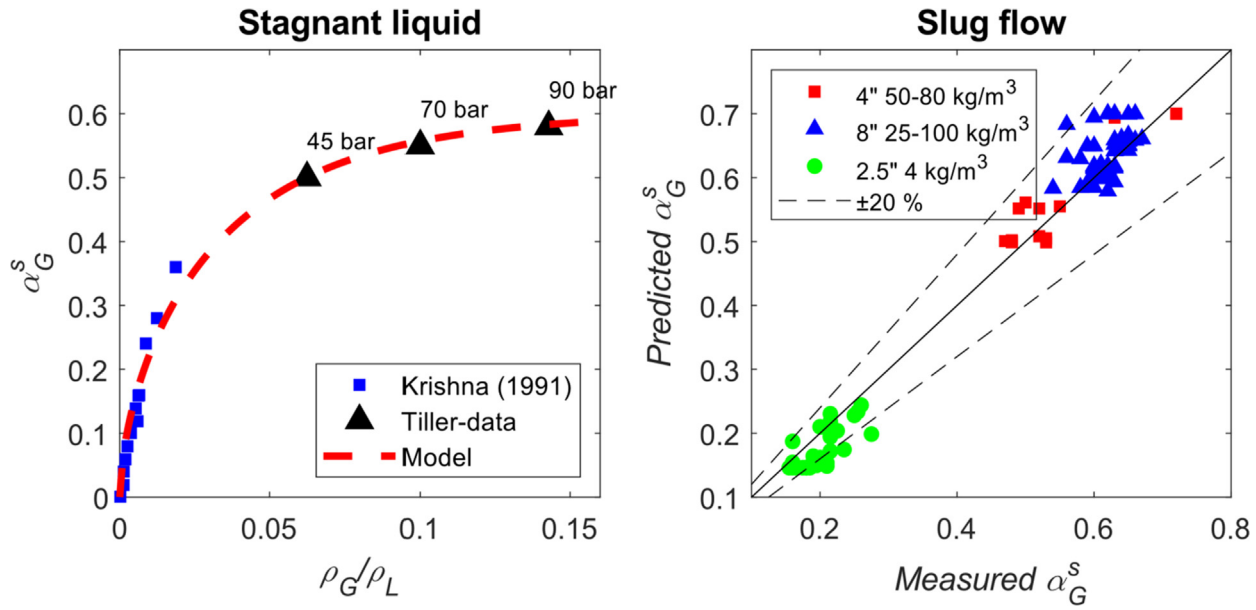

Fig. 7. Comparison of Eq. (18) with experiments in stagnant liquid (left) and slug flow (right). The graphs are taken from (Kjølaas et al., 2017).

liquid for various gas/liquid density ratios. In this plot, because the liquid is stagnant, only the first term of Eq. (18) contributes. In the right graph Eq. (18) is compared to measured slug gas fractions for three different vertical slug flow data sets with a wide range of pipe diameters and gas densities. For the data presented here, both terms in Eq. (18) generally contribute. At high pressure, however, the first term tends to be the dominant one.

In the current implementation, we have placed an upper limit of 0.7 on α_G^S because we have not observed slug gas fractions exceeding this value. In addition, the expression inside the square root sign in Eq. (18) must obviously be limited to non-negative values.

By using Eqs. (2), (17) and (18), we can calculate all the terms on the right-hand-side of Eq. (15), yielding the average gas fraction in churn/slug flow.

3.1.3. Unified model

Sections 3.1.1 and 3.1.2 describe how we can model bubbly flow and churn/slug flow, respectively. In a unified framework, we must select the appropriate model based on some physical criterion, meaning that we must have a way to identify the transition between bubbly flow and churn/slug flow. In the UCM framework, this transition takes place when the slug fraction *SF* equals unity, and we may use this fact to find the critical conditions for this transition by substituting *SF = 1* into Eq. (9), which then yields:

$$USG = \alpha_G^S U_G^S \tag{19}$$

The implication is that if $\alpha_G^S U_G^S$ exceeds the global superficial gas velocity *USG*, then the flow regime is bubbly flow. Otherwise, it is churn/slug flow, or possibly annular flow. We have not included an annular flow model in our framework, so a prerequisite for using this framework is that the flow is not annular, and we have thus selected the experimental data accordingly. An example showing the bubbly-churn/slug flow regime transition is shown in Fig. 8, where we have plotted the gas holdup versus *USG*, using two different markers to distinguish between the two flow regimes. The green triangles represent the slug gas fraction, which is relatively high due to the high pressure in the experiments.

We observe in this graph that the slug gas fraction remains constant for sufficiently low gas rates (below 1.2 m/s). In this range, only the first term in Eq. (18) contributes. Beyond this point, the slug gas fraction increases slightly, and this is caused by the second term in (18). The model is however clearly dominated by the first term at these high-pressure conditions.

In Fig. 9 we show the two-phase data points (gas/oil and gas/water) from the experiments presented in Section 2, where the liquid fraction α_L is plotted against the superficial liquid velocity *USL*. The markers show the measured values, and the lines represent predictions obtained using the unified bubbly/churn/slug model described in this section. Non-filled markers are used for the experimental points for which bubbly flow is predicted, and filled markers are used for the churn/slug regime. The agreement between the model and the measurements is very good, suggesting that this two-phase model is a good starting point for modelling three-phase vertical flows, which we will address in the next section.

3.2. Generalization to three-phase flows

In this section we aim to adapt the two-phase model outlined in the previous section to predict three-phase vertical flows. To do this, we must make certain assumptions about how the oil and water is distributed in vertical flows. In Section 2.4.1, we found that the slip velocity between oil and water is generally small. We believe that the reason for these small oil/water slip velocities is that the oil and water is close to homogeneously mixed, either as water droplets in the oil or vice versa. Indeed, in vertical steady-state flows, the force of gravity does not contribute to phase separation, so any separation must be a product of some other phenomena, such as turbophoresis (Caporaloni et al., 1975; Young and Leeming, 1997; Uijttewaal and Oliemans, 1996). Such effects tend to be quite weak, especially if the density difference is small (Reeks, 1983), hence we should expect the oil and water to be well mixed.

The assumption of fully mixed oil/water greatly simplifies the modelling of three-phase flows because we can treat the oil/water mixture as a liquid with some appropriate mixture properties. The liquid mixture density ρ_L is simply given by:

$$\rho_L = WC \cdot \rho_W + (1 - WC) \cdot \rho_O \tag{20}$$

The viscosity is not a parameter in our model, so we do not need to define a liquid mixture viscosity. The surface tension is however used in some of the selected closure laws, so we do need to define a "mixing rule" for that parameter. Here, we have elected to define

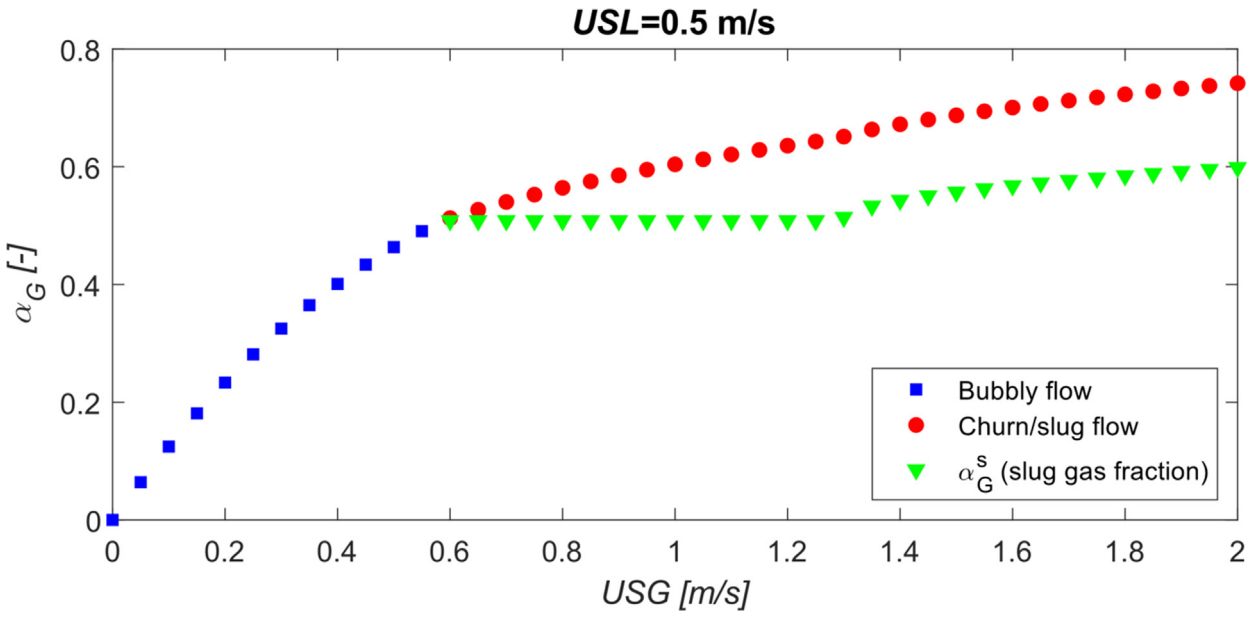

Fig. 8. Predicted gas holdup plotted versus the superficial gas velocity *USG* for *USL* = 0.5 m/s and WC = 0%. The green triangles represent the slug gas fraction. (For interpretation of the references to colour in this figure legend, the reader is referred to the web version of this article.)

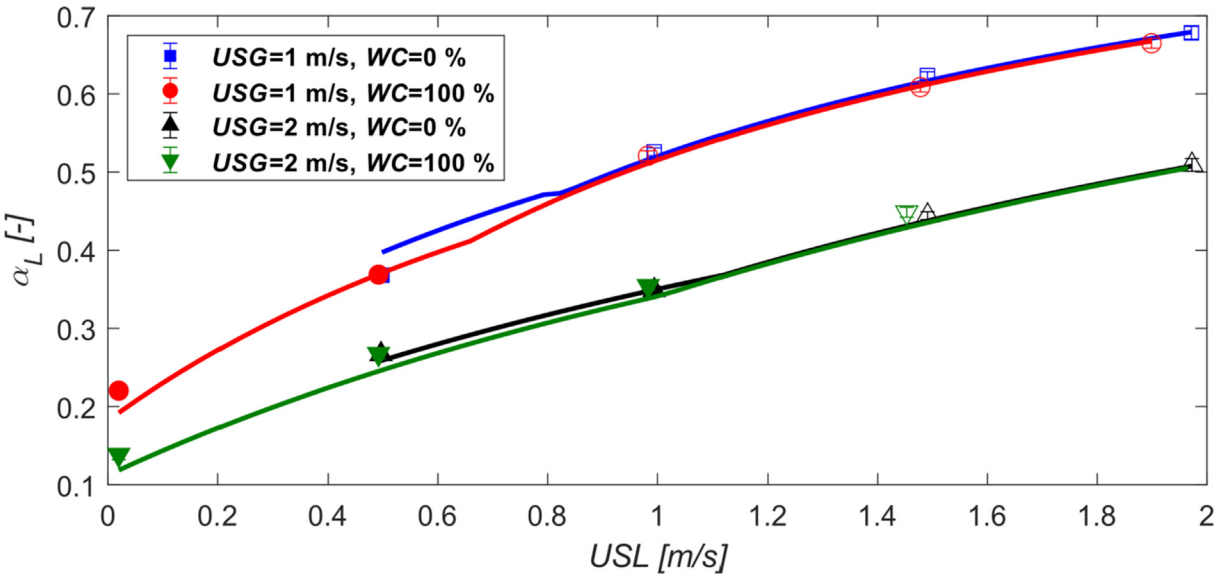

Fig. 9. Liquid holdup plotted versus the superficial liquid velocity *USL* for *USG* = 1 and 2 m/s, and *WC* = 0 and 100%. The markers are the measured values (non-filled markers = bubbly flow), and the lines were generated using the unified model described in this section.

the liquid mixture surface tension σ_{GL} as simply being the surface tension of the continuous liquid phase since we are assuming that the gas bubbles are dispersed in that phase.

With these simple definitions in place, we may readily deploy the two-phase model proposed in Section 3.1 on three-phase vertical flows. Fig. 10 shows the associated results, where the liquid holdup is plotted versus the water cut for the various cases. The markers represent the measured values (non-filled = bubbly flow), and the lines represent the model results. We observe that the predictions are good for *WC* = 0% and *WC* = 100%, which is expected since these are the same points that were included in Fig. 9. For intermediate water cuts, however, the model is unable to match the measurements. It is thus clear from these graphs that generalizing the model to three-phase flows requires something more than just introducing some liquid mixture properties.

We have inferred from the data that the liquids are well mixed in three-phase flows, and the liquid mixture can thus be assumed to be made up of liquid droplets dispersed inside a continuous phase. Specifically, at low water cuts, the liquid is presumably an oil-continuous mixture with water droplets, while at high water cuts, it should be a water-continuous mixture with oil droplets. The point at which the transition between oil-continuous and water continuous flow takes place is usually referred to as the phase inversion point. In Section 2.2, we deduced from the mini-loop experiments that phase inversion takes place at a water cut of about 40%.

In addition to the oil- or water droplets there will be bubbles inside the continuous liquid, at least inside liquid slugs. Fig. 11 provides illustrations of the two- and three-phase mixtures in slugs, where the yellow circles represent gas bubbles, the brown circles represent liquid droplets, and the blue background is the continuous liquid phase.

To explain the observed water cut dependency on the liquid fraction, we must return to the physical interpretation of the

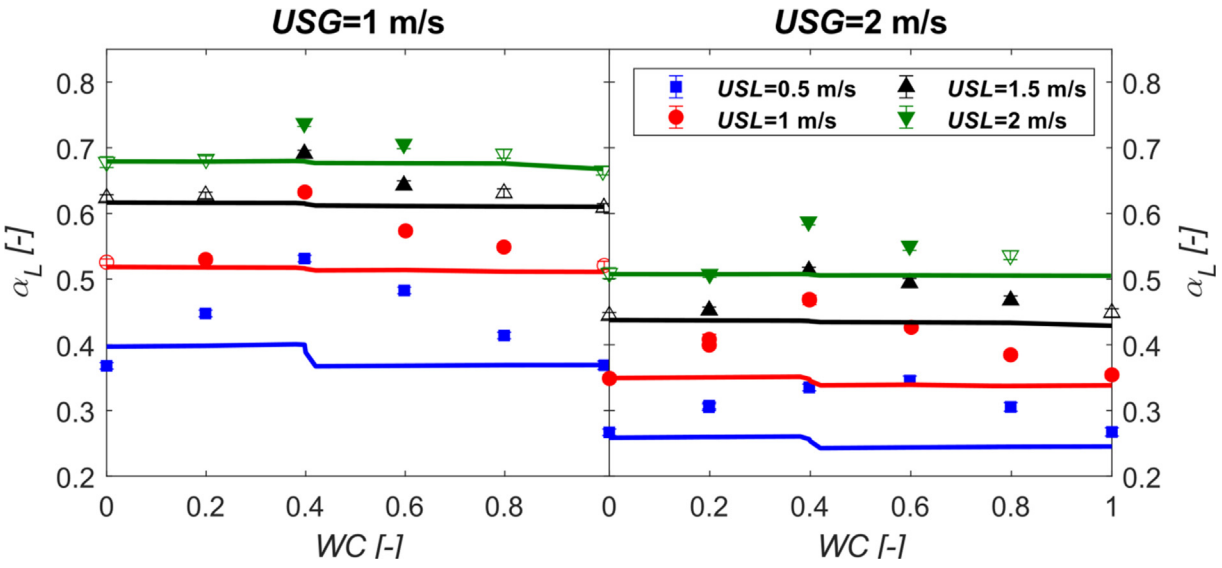

Fig. 10. Liquid holdup plotted versus the water cut *WC* for *USG* = 1 and 2 m/s, and *USL* = 0.5–2 m/s. The markers are the measured data (non-filled markers = bubbly flow), and the lines were generated using the model described in Section 3.1.

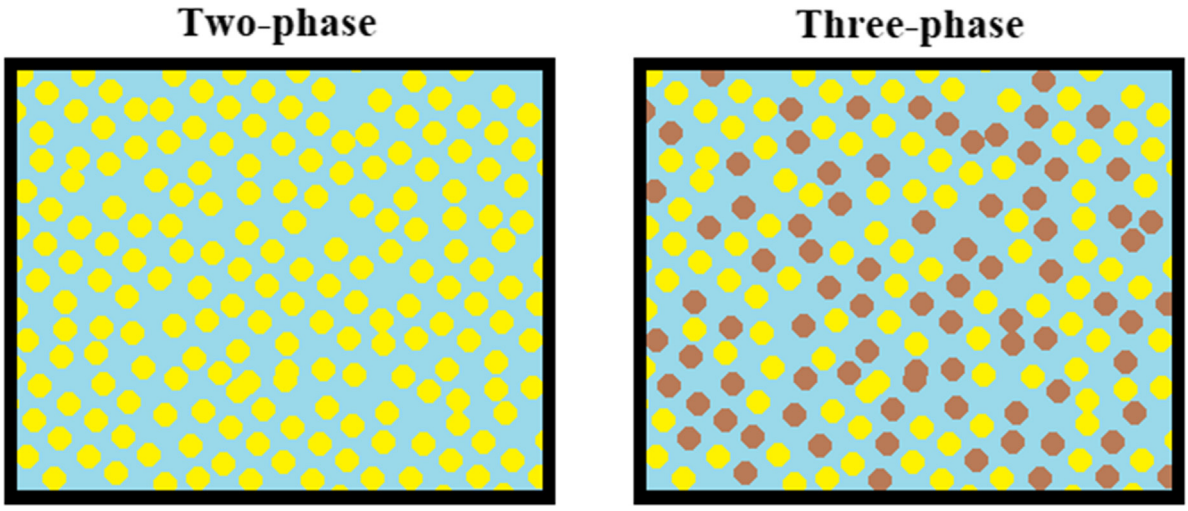

Fig. 11. Schematic illustrations of liquid slugs in two- and three-phase flows. The blue represents the continuous liquid, the yellow circles represent gas bubbles, and the brown circles represent liquid droplets. (For interpretation of the references to colour in this figure legend, the reader is referred to the web version of this article.)

model for the gas fraction in slugs in vertical flow. As noted in Section 3.1.2, the underlying idea behind the gas entrainment model is that the concentration of bubbles in the slugs is determined by the maximum stable concentration of bubbles. The model that we have used to calculate the maximum bubble concentration is given by Eq. (18), but this model was exclusively developed based on two-phase gas–liquid flows.

As we may deduce from the simple illustrations shown in Fig. 11, we should expect that a liquid that contains a lot of liquid droplets must have less available capacity for storing gas bubbles, simply because gas bubbles and liquid droplets can presumably not occupy the same space. Consequently, we should expect the gas fraction inside the slugs to decrease as the liquid droplet concentration increases. The maximum liquid droplet concentration is obtained at the inversion point, where the liquid changes from oil- to water continuous, so this is where we may expect to have the lowest gas bubble concentration. This fits well with the observed trends in the liquid fraction, where the maximum liquid fraction was obtained at *WC* = 40%. Based on this simple idea, we propose the following correction to Eq. (18):

$$\alpha_G^S = \max\left(\alpha_{G,2-phase}^S - C_d, 0\right) \tag{21}$$

Here, $\alpha_{G,2-phase}^S$ is the two-phase model given by Eq. (18), and C_d is the liquid droplet concentration. Assuming no oil/water slip, C_d equals the water cut *WC* below the inversion point, while above the inversion point, C_d equals *1-WC*. The physical interpretation of this correction is that the model given by Eq. (18) provides the maximum concentration of bubbles *and* droplets combined. By introducing this simple correction to our model, we obtain the results shown in Fig. 12, where we have again plotted the liquid fraction against the water cut. Here, the dashed lines are the results obtained *without* the three-phase correction, while the solid lines represent the results *with* this correction. The trends observed in the measurements are matched very well with the new model, and the overall agreement is much better than without the three-phase correction.

We did also try a slightly different formulation/assumption for the generalization to three-phase flows. In the alternative formulation we assumed that the concentration of gas bubbles in the continuous liquid phase (between the droplets) remained the same in

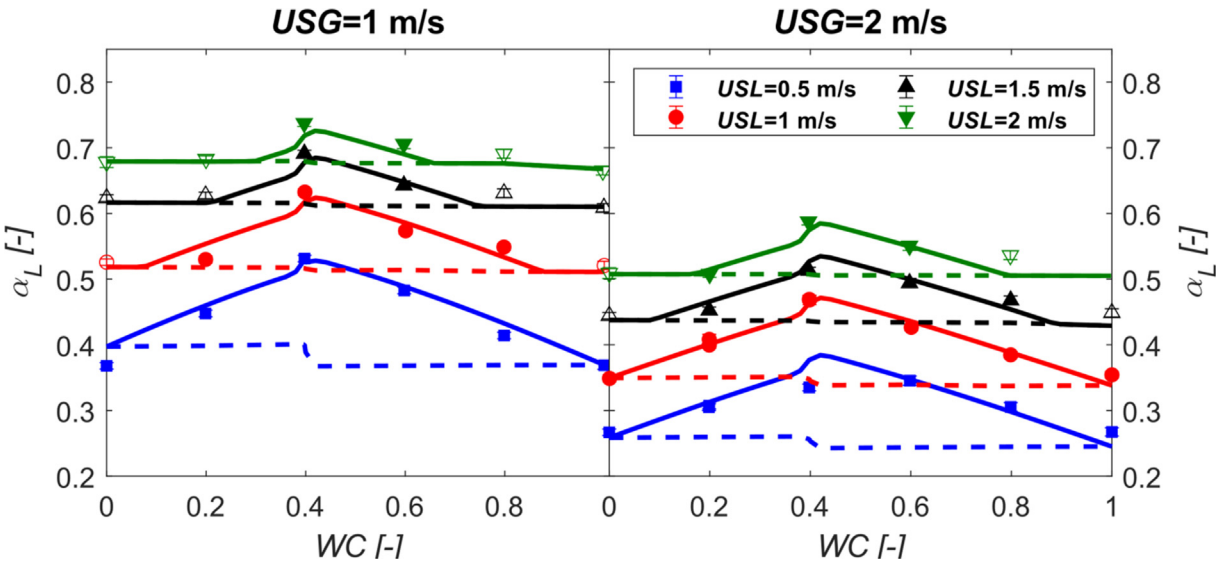

Fig. 12. Liquid holdup plotted versus the water cut *WC* for *USG* = 1 and 2 m/s, and *USL* = 0.5–2 m/s. The markers are the measured data (non-filled markers = bubbly flow), the dashed lines were generated by the model without the three-phase correction, and the solid lines were generated after including the three-phase correction.

two- and three-phase flows, leading to the following expression: $\alpha_G^S = \alpha_{G,2-phase}^S(1 - C_d)$. Although this formulation yields qualitatively similar results as (21), we ultimately found that Eq. (21) gave a better match with the experimental data.

It is worth noting that the proposed three-phase correction does not include any additional tuneable model coefficients, which is a positive feature. Indeed, one often finds that model coefficients have limited ranges of applicability, so introducing as few new model coefficients as possible is generally a virtue in model development.

We should also point out that the proposed model improvement has most impact at high gas densities, since slug gas fractions tend to be much higher at high gas densities than at low gas densities, see Fig. 7. Consequently, in most laboratory experiments described in the literature, where the system pressure tends to be near-atmospheric (Descamps et al., 2007; Colmanetti et al., 2018; Xu et al., 2012; Frechou, 1986), the three-phase effect described here will typically have a limited impact.

Fig. 13 shows the bubbly/slug flow transition for different water cuts according to the proposed model (using Eq. (19)). Here, the regions above the lines are the bubbly flow domains. As expected, we observe that for two-phase flows (*WC* = 0% and 100%), the bubbly flow region is very large. Meanwhile, as the water cut approaches the inversion point (40%), the bubbly flow region diminishes.

4. Application of model on field data

In this section we show the impact of the modification of the void-in-slug model for an oil field operated by TotalEnergies in the Gulf of Guinea. For confidentiality reasons, we cannot disclose the name of the field, but we will provide a brief description.

The oil field consists of a 11.5 km long near-horizontal flowline ending up in an 810 m riser with an internal diameter of 0.254 m. In order to reduce the gravitational pressure drop in the riser, gas is injected 200 m upstream of the riser base. In the current data set, the gas lift flow rate was varied in steps over 6 days to find its optimal setting, see Fig. 14. Each step was sufficiently long to achieve steady state. In all the experiments, the water cut was equal to 16%, leading to a water-in-oil emulsion. The produced oil and water rates were equal to 2544 Sm^3/d and 402 Sm^3/d, respectively, while the gas rate out of the well was 417 kSm^3/d. Meanwhile, the gas lift flow rate was varied between 202 and 427 kSm^3/d. The first stage separator was operated between 22 and 25 bar, and the pressure drop at the riser base varied between 39 and 41 bar. This means that there is a strong pressure drop over the riser, resulting in a strong gas expansion over the riser. The mixture velocity varied between 3.3 and 8.1 m/s at the lowest gas lift flow rate, and between 3.8 and 9.2 m/s at the highest gas lift flow rate. The temperature was not measured in the riser, but it was measured upstream. Based on temperature calculations, the temperatures were in the range 47–58 °C in the riser. With these pressure and temperature ranges, the gas density varied between 18 and 32 kg/m^3 and the oil density between 773 and 791 kg/m^3. The oil viscosity varied between 1.2 and 1.5 mPa s. The liquid mixture Reynolds numbers were found to be well above 10000, which is well into the turbulent regime.

Because of the gas expansion and the change of fluid properties along the riser, the riser must be discretized in small sections to predict the total pressure drop. Here, we used the LedaFlow software to calculate the evolution of the pressure and temperature (and the associated changes in the fluid properties) along the riser. LedaFlow is a software based on transient 1D models for three-phase flow in pipes and is used in the oil & gas industry to predict the pressure drop, the hold-up and the temperature in production systems ("LedaFlow," Kongsberg Digital AS, xxxx). In the current demonstration, we show results obtained using LedaFlow versions 2.6 and 2.7. In turbulent bubbly/churn/slug flow in vertical pipes, LedaFlow 2.6 essentially uses the closure laws described in this paper, except for the proposed three-phase correction described by Eq. (21). LedaFlow 2.7 on the other hand does include Eq. (21), and thus typically yields higher pressure drop in near-vertical three-phase flows compared to LedaFlow 2.6.

Fig. 14 shows the pressure drop over the riser plotted versus time. The thick black lines are the average measured values during the various time intervals, while the thin green and red lines are predictions obtained from LedaFlow versions 2.6 and 2.7, respectively. The blue line shows the gas lift flow rate, which is decreased in discrete steps. We observe in this graph that LedaFlow 2.6 systematically underpredicts the total pressure drop over the riser for all the gas lift flow rates. On the other hand, LedaFlow 2.7, which includes Eq. (21), predicts pressure drops that are in very good agreement with the measured data. This comparison shows that including this newly discovered three-phase effect can have important practical implications for high-pressure production sys-

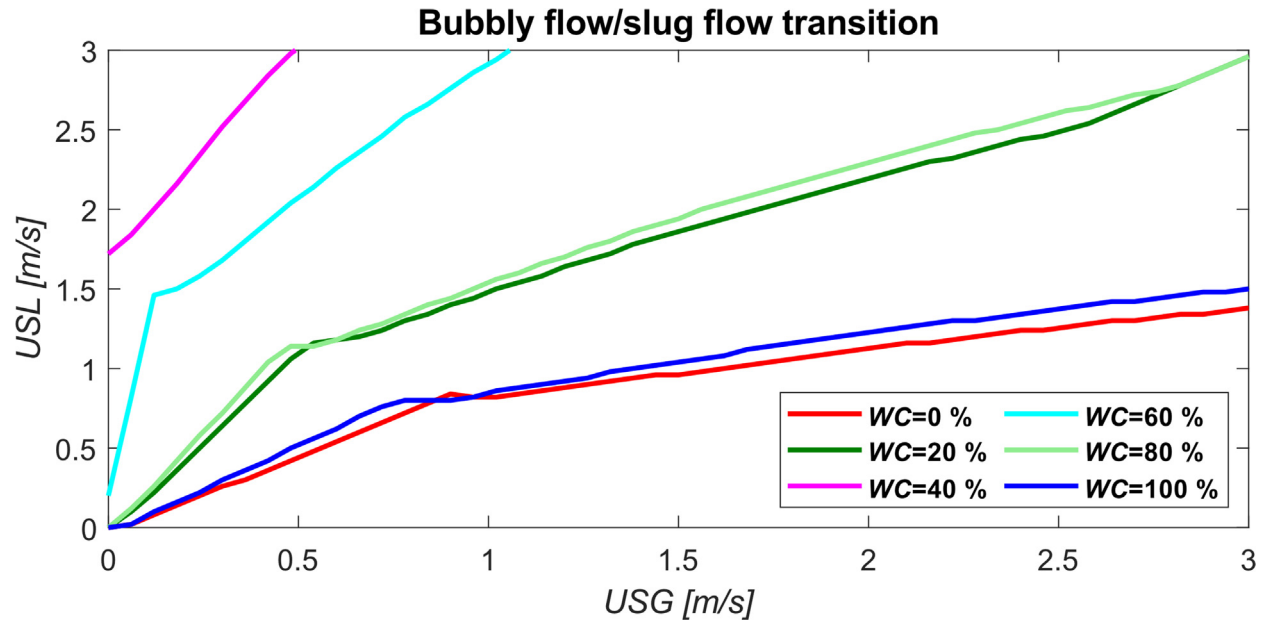

Fig. 13. Lines showing the bubbly/slug flow transition for different water cuts according to the proposed model. The region above the lines is bubbly flow.

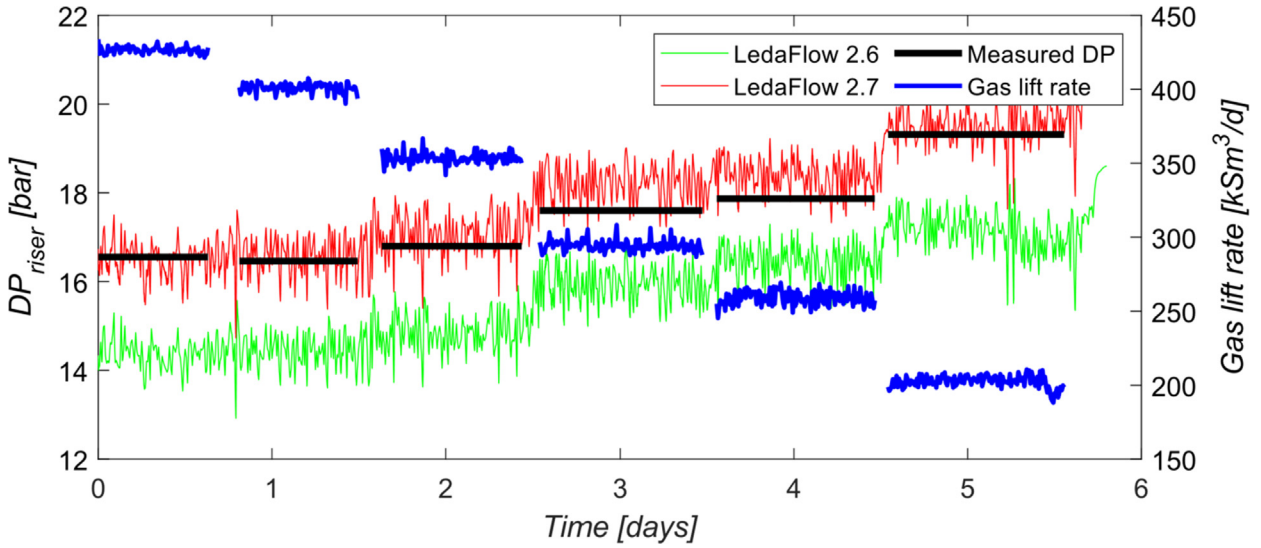

Fig. 14. Pressure drop and gas lift rate in the riser plotted against time.

tems with risers, and that the exclusion of this effect can yield significant prediction errors.

5. Conclusions

A set of two- and three-phase experiments were conducted in a 50 m long 4″ vertical pipe using nitrogen, Exxsol D60 and water. The results showed that the liquid content and pressure drop was highly sensitive to the injected water cut.

A combined bubbly/slug/churn flow model was implemented in a unit cell model framework, using closure laws from the public literature that were developed for two-phase gas–liquid flows. The resulting model was able to predict the two-phase experiments well but showed significant under-prediction of the liquid fraction in three-phase flows.

Our proposed explanation for the observed three-phase effects is that the presence of liquid droplets constrains the gas bubble capacity of the liquid so that the concentration of small bubbles inside the liquid becomes smaller in three-phase flows than in two-phase flows. The gas entrainment closure law used in the implemented model framework was thus amended to account for this mechanism. The prevailing predictions showed that the observed three-phase effects could be reproduced very accurately using this simple assumption, without having to introduce any additional model coefficients.

CRediT authorship contribution statement

Jørn Kjølaas: Conceptualization, Validation, Methodology, Software, Investigation, Data curation, Writing – original draft, Visualization, Supervision. **Roel Belt:** Conceptualization, Methodology, Resources, Writing – review & editing, Supervision. **Marita Wolden:** Methodology, Investigation, Writing – review & editing, Project administration, Supervision. **Heiner Schumann:** Methodology, Investigation, Writing – review & editing. **Vanessa Richon:** Conceptualization, Resources, Writing – review & editing, Supervision, Funding acquisition, Project administration.

Declaration of Competing Interest

The authors declare that they have no known competing financial interests or personal relationships that could have appeared to influence the work reported in this paper.

Acknowledgements

We would like to extend our gratitude to TotalEnergies for financing the experimental campaign reported in this paper.

The authors would also like thank LedaFlow Technologies DA (owned by SINTEF, Kongsberg Digital, TotalEnergies and ConocoPhillips) and the The Research Council of Norway (grant number 281881), for financing the model development described here.

Finally, we want to thank all the scientific and technical personnel at the SINTEF Multiphase Laboratory for all their dedicated work on the experiments.

Appendix A. Experimental data

Table 4

Table 4
Tabulated experimental data: Superficial gas velocity *USG*, superficial liquid velocity *USL*, water cut *WC*, liquid holdup α_L, water holdup α_W, pressure drop *-dp/dx*. Some cells are empty because the associated measurement was either not conducted or conducted unsuccessfully.

USG [m/s]	USL [m/s]	WC [-]	α_L [-]	α_W [-]	-dp/dx [Pa/m]
0.989	1.485	0.397	0.691	0.277	6547
0.989	1.973	0.798	0.691		7138
0.990	1.477	0.798	0.631		6474
0.990	1.899	0.997	0.665	0.665	7266
0.990	1.976	0.597	0.706		6977
0.990	1.980	0.397	0.737	0.290	7101
0.990	1.481	0.597	0.643		6368
0.991	1.970	0.200	0.683	0.139	6123
0.991	0.495	0.398	0.531	0.212	4915
0.991	1.487	0.199	0.627	0.136	5567
0.991	1.972	0.000	0.678	0.000	5917
0.991	0.990	0.398	0.633	0.256	5889
0.991	0.984	0.798	0.549	0.440	5607
0.991	0.983	1.000	0.521	0.521	5693
0.991	1.478	0.999	0.609	0.609	6640
0.992	1.491	0.000	0.623	0.000	5350
0.992	0.994	0.601	0.574	0.344	5606
0.992	0.495	0.598	0.483	0.286	4682
0.992	0.991	0.199	0.530	0.122	4767
0.993	0.494	0.799	0.414	0.328	4293
0.993	0.498	0.000	0.368	0.000	3313
0.993	0.492	1.000	0.369	0.369	4146
0.993	0.994	0.000	0.526	0.000	4534
0.993	0.496	0.199	0.448	0.116	4010
0.996	0.020	1.000	0.220	0.220	2457
1.977	1.965	0.998			6166
1.981	1.973	0.396	0.588	0.231	6161
1.981	1.972	0.798	0.536		5978
1.982	1.970	0.200	0.508	0.106	5025
1.982	1.976	0.597	0.551		5912
1.982	1.478	0.799	0.468		5207
1.983	1.482	0.597	0.494		5286
1.984	1.973	0.000	0.509	0.000	4905
1.984	1.485	0.397	0.513	0.215	5123
1.984	1.453	1.000	0.449	0.449	5272
1.985	0.994	0.601	0.427	0.261	4554
1.985	0.990	0.398	0.468		4737
1.985	0.983	1.000	0.354	0.354	4256
1.985	0.985	0.799	0.385	0.311	4328
1.986	0.991	0.398	0.469	0.190	4763
1.986	1.491	0.000	0.444	0.000	4252
1.986	1.488	0.199	0.453	0.099	4458
1.986	0.991	0.199	0.400	0.095	3851
1.987	0.991	0.199	0.408		3854
1.987	0.495	0.598	0.346		3568
1.987	0.994	0.000	0.349	0.000	3423
1.987	0.494	0.799	0.306		3373
1.988	0.495	0.398	0.335	0.151	3379
1.988	0.492	1.000	0.267	0.267	3213
1.989	0.497	0.198	0.305	0.080	2972
1.989	0.496	0.199	0.308	0.079	2971
1.989	0.496	0.000	0.267	0.000	2657
1.993	0.020	1.000	0.138	0.138	1720

References

Zuber, N., Findlay, J., 1965. Average Volumetric Concentration in Two-Phase Flow Systems. J. Heat Transfer 87, 453–468. https://doi.org/10.1115/1.3689137.

Shi, H., Holmes, J., Diaz, L., Durlofsky, L.J., Aziz, K., 2005. Drift-Flux Parameters for Three-Phase Steady-State Flow in Wellbores. SPE J. 10 (02), 10(2), 130–137. https://doi.org/10.2118/89836-pa.

Pietrzak, M., Płaczek, M., Witczak, S., 2017. Upward flow of air-oil-water mixture in vertical pipe. Exp. Therm Fluid Sci. 81, 175–186.

Dukler, A.E., Hubbard, M.G., 1975. A Model for Gas-Liquid Slug Flow in Horizontal and Near Horizontal Tubes. Ind. Eng. Chem. Fundam. 14 (4), 337–347.

Fernandes, R.C., Semiat, R., Dukler, A.E., 1983. Hydrodynamic model for gas-liquid slug flow in vertical tubes. AIChE J. 29 (6), 981–989. https://doi.org/10.1002/(ISSN)1547-590510.1002/aic.v29:610.1002/aic.690290617.

Fabre, J., Liné, A., 1992. Modeling of two-phase slug flow. Ann. Rev. Fluid Mech. 24 (1), 21–46. https://doi.org/10.1146/annurev.fl.24.010192.000321.

Guet, S., Decarre, S., Henriot, V., Liné, A., 2006. Void fraction in vertical gas–liquid slug flow: Influence of liquid slug content. Chem. Eng. Sci. 61 (22), 7336–7350. https://doi.org/10.1016/j.ces.2006.08.029.

Kjølaas, J., Shmueli, A., Morin, A., Belt, R., 2017. "Improvement of LedaFlow for churn flow in vertical pipes", in *18th International Conference on Multiphase Technology*. Cannes, France.

Descamps, M., Oliemans, R., Ooms, G., Mudde, R., 2007. Experimental investigation of three-phase flow in a vertical pipe: Local characteristics of the gas phase for gas-lift conditions. Int. J. Multiphase Flow 33 (11), 1205–1221. https://doi.org/10.1016/j.ijmultiphaseflow.2007.06.001.

Colmanetti, A.R.A., de Castro, M.S., Barbosa, M.C., Rodriguez, O.M.H., 2018. Phase inversion phenomena in vertical three-phase flow: Experimental study on the influence of fluids viscosity, duct geometry and gas flow rate. Chem. Eng. Sci. 189, 245–259. https://doi.org/10.1016/j.ces.2018.05.050.

Xu, J.-y., Zhang, J., Liu, H.-F., Wu, Y.-X., 2012. Oil–gas–water three-phase upward flow through a vertical pipe: Influence of gas injection on the pressure gradient. International Journal of Multiphase Flow 46 46, 1–8.

Frechou, D., 1986. Etude de l'écoulement ascendant à trois fluides en conduite verticale, Toulouse. These Inst. Natl. Polytech, France.

Collins, R., Moraes, F.F.D., Davidson, J.F., Harrison, D., 1978. The motion of a large gas bubble rising through liquid flowing in a tube. JFM 89 (3), 497–514.

Boucher, A., Belt, R., Liné, A., 2021. "Review of potential flow solutions for velocity and shape of long isolated bubbles in vertical pipes.", *Accepted for publication in*. Rev. Chem. Eng.

"National Institute of Standards and Technology," [Online]. Available: http://webbook.nist.gov/chemistry/fluid/.

Pal, R., 1993. Pipeline Flow of Unstable and Surfactant-Stabilized Emulsions. AIChE J. 39 (11), 1754–1764.

Hewitt, G.F., Jayanti, S., 1993. To churn or not to churn. Int. J. Multiphase Flow 19 (3), 527–529.

Mao, Z.S., Dukler, A.E., 1993. The myth of churn flow? Int. J. Multiphase Flow 19 (2), 377–383.

Taitel, Y., Barnea, D., Dukler, A., 1980. Modeling flow pattern transitions for steady upward gas–liquid flow in vertical tubes. AIChE J.3 3, 345–354.

Nicklin, D., Wilkes, J., Davidson, J., 1962. Two phase flow in vertical tubes. Trans Inst Chem Engs., 61–68

Krishna, R., Wilkinson, P.M., 1991. A model for gas holdup in bubble columns incorporating the influence of gas density on flow regime transitions. Chem. Eng. Sci. 46 (10), 2491–2496.

Krishna, R., 2000. "A Scale-up Strategy for a Commercial Scale Bubble Column Slurry Reactor for Fischer-Tropsch Synthesis", *Oil & Gas Science and Technology – Rev*. IFP 55 (4), 359–393.

Harmathy, T.Z., 1960. Velocity of large drops and bubbles in media of infinite or restricted extent. AIChE J. 6 (2), 281–288.

Richardson, J.F., Zaki, W.N., 1954. Sedimentation and fluidisation. Part 1. Trans. Inst. Chem. Eng. 32, 35–53.

Ishii, M., Zuber, N., 1979. Drag coefficient and relative velocity in bubbly, droplet or particulate flows. AIChE J. 25, 843–855. https://doi.org/10.1002/aic.690250513.

Joseph, D.D., 2003. Rise velocity of a spherical cap bubble. J. Fluid Mech. 488, 213–223.

Caporaloni, M., Tampieri, F., Trombetti, F., Vittori, O., 1975. Transfer of particles in nonisotropic air turbulence. J. Atmos. Sci. 32 (3), 565–568.

Young, John, Leeming, Angus, 1997. A theory of particle deposition in turbulent pipe flow. JFM 340, 129–159.

Uijttewaal, W., Oliemans, R., 1996. Particle dispersion and deposition in direct numerical and large eddy simulations in vertical pipe flows. Phys. Fluids 8, 2590–2604.

Reeks, M.W., 1983. The transport of discrete particles in inhomogeneous turbulence. J. Aerosol Sci. 14 (6), 729–739.

"LedaFlow," Kongsberg Digital AS, [Online]. Available: http://www.ledaflow.com/. [Accessed 24 June 2020].